Samokhin, Sergey; Hyytiä, Jari; Zenger, Kai; Ranta, Olli; Blomstedt, Otto; Larmi, Martti

Adaptive Boost Pressure Control for Four-Stroke Diesel Engine Marine Application in the Presence of Dynamic Uncertainties

Published in:
IEEE Transactions on Control Systems Technology

DOI:
10.1109/TCST.2017.2768425

Published: 01/01/2019

Document Version
Peer-reviewed accepted author manuscript, also known as Final accepted manuscript or Post-print

Please cite the original version:
Samokhin, S., Hyytiä, J., Zenger, K., Ranta, O., Blomstedt, O., & Larmi, M. (2019). Adaptive Boost Pressure Control for Four-Stroke Diesel Engine Marine Application in the Presence of Dynamic Uncertainties. *IEEE Transactions on Control Systems Technology*, *27*(1), 221-233. Article 8110844.
https://doi.org/10.1109/TCST.2017.2768425

Adaptive boost pressure control for four-stroke diesel engine marine application in presence of dynamic uncertainties

Sergey Samokhin, Jari Hyytiä, Kai Zenger, Olli Ranta, Otto Blomstedt, and Martti Larmi

Abstract—**Robustness of the control system in marine engines with respect to its time-varying dynamics has recently become an important research topic. The variation of dynamics, caused primarily by the mechanical wear of components or their faults originating from tough operating condition, can lead to the overall control system instability (or marginal stability, depending on how severe the variation is). The biggest issue is that the marine engines cannot always be fixed fast enough (especially on large cargo vessels, spending hundreds of hours cruising). In this work, a control adaptation (indirect model-reference adaptive control) is proposed to deal with the engine parameter variation in a way that the original system response is preserved. The stability and robustness of the proposed control system are studied by means of numerical simulations. Finally, the performance of the control concept is validated on the medium-speed diesel engine testbed at constant speed under load transients. Superior performance compared to fixed-parameter PI-control is demonstrated.**

Index Terms—**Diesel engine, adaptive control, mechanical wear, MRAC, robustness, experimental evaluation.**

I. Introduction

The parameter variation of internal combustion engines throughout their life-cycle represents additional complexity for automatic control systems. Such variation can typically originate from the mechanical wear and tear of engine components (e.g., natural or caused by external disturbance, including rough seas [1]). Thus, the resultant engine dynamics may become significantly different from the nominal ones leading to the overall degraded engine performance, including increased fuel consumption and emission production and in the worst case rough running, hunting or stalling. These problems occur due to inability of controllers with fixed tuning parameters (e.g., classical proportional-integral (PI) controllers) to provide predefined engine performance for the process with updated dynamics, including, for example, altered transient response (slower/faster rise- and settling time, gain variations), measurement delay and actuator stiction [2], [3].

As the environmental regulations imposed by the international maritime organization (IMO) are getting increasingly stringent [4], the problem of the control system adaptation to time-varying engine dynamics has recently become an important topic among the marine engine manufacturers and several large-scale research projects have been established [5], [6]. Such time-varying dynamics or parameters caused by the mechanical wear or aging of engine components is essentially a relatively slow process. While still being undesirable and obviously capable of causing control issues (e.g., poor reference tracking), such variation of parameters is a minor issue for the automotive industry, where the faulty components can be replaced relatively quick and easy. However, this is not the case for marine industry where large cargo vessels can spend hundreds of hours sailing in the sea [7], [8] and the immediate maintenance is not always possible. Moreover, an on-the-spot maintenance might require to bring vessel to a full stop, which can cause safety issues, especially if on busy routes [9], [10]. Additional issues for marine diesel engines come from their typical driving cycle which is significantly different to the one of the automotive engines [7]. While full load conditions for a city car can typically occur during rapid acceleration, some of the marine engines spend a large part of their operating time in such conditions (e.g., 75-90% load for large two-stroke engines) [11]. Consequently, the engine components experience increased levels of stress as compared to the automotive engines and the operating parameters can change as a result. It can be concluded that the marine engines are subjects to considerably less dynamic operation in comparison to the automotive engines but are operated heavily for prolonged periods of time.

One popular way of dealing with the problem of parameter variation is to utilize the robust control approach which takes into account process uncertainties [12]. Although very powerful, this approach inevitably compromises the closed-loop response of the engine under nominal conditions in order to provide the desired robustness margin and keep it stable in case of parameter variation.

A different approach to solving this problem is to

Manuscript was submitted for review February 13, 2017; revised September 6, 2017; accepted October 22, 2017. This work was supported by European Commission, DG Research, under Contract SCP1-GA-2011-284354.

S. Samokhin and K. Zenger are with the Department of Electrical Engineering and Automation, Aalto University, Maarintie 8, 02150 Espoo, Finland (e-mail: sergey.samokhin@aalto.fi, kai.zenger@aalto.fi).

J. Hyytiä, O. Ranta, O. Blomstedt and M. Larmi are with the Department of Mechanical Engineering Engineering, Aalto University, Puumiehenkuja 5 A, 02150 Espoo, Finland (e-mail: jari.hyytia@aalto.fi, olli.ranta@aalto.fi, otto.blomstedt@aalto.fi, martti.larmi@aalto.fi).

design a controller which provides desired performance for the nominal case and then to adapt its parameters accordingly if the engine behavior changes. In this work, a solution is provided by the class of controllers known as model reference adaptive control (MRAC) which utilizes a linear model of the desired closed-loop response and updates the control parameters in a way that this response is maintained whenever possible. Specifically, indirect version of MRAC is implemented which includes both controller and identifier and allows for flexibility in choosing schemes for their implementation [13].

To the authors' knowledge very few publication have addressed the problem of control adaptation within the marine industry. These include control adaptation to varying measurement delay of UEGO sensor in adaptive closed-loop lambda control [14], adaptive engine speed control where the adaptation to uncertain load changes is considered [15] and nonlinear adaptive control of exhaust gas recirculation (EGR) [16], [17]. Nevertheless, a variety of approaches to the adaptation of controller parameters has been studied within the automotive industry. However, as mentioned above, the components degradation is not the biggest issue for automotive engines and, therefore, the adaptive control has been viewed from another perspective. Mostly, adaptation to variation of engine dynamics at different operating points (OP) has been evaluated. These include adaptive and learning controllers [18], model predictive control with the adaptation of model time-delays at different engine OP [19], adaptive parameter estimation for feedforward control [20], adaptive internal model control for boost pressure regulation [21].

In this work, the goal is to evaluate the possibility of control adaptation to changes in engine dynamics due to mechanical wear or aging of components. Such wear or aging is essentially a very slow process and, in practice, is suitable for adaptive controllers which work best with slowly time-varying processes. While there are many moving components that can be affected by mechanical wear, we choose to demonstrate the adaptation on the example of a degraded actuator of the variable geometry turbocharger (VGT). The actuator degradation is implemented numerically rather than physically in order to allow for repeatable and reliable testing and avoid extra costs related to the actuator damage. We point out that the indirect MRAC does not require specific information on the fault origins, type, size, etc., and therefore the case study carried out in this work can be easily translated on faults other than the VGT actuator dynamics variation.

The verification and tuning of the adaptive controller is done via numerical simulations in Matlab/Simulink with the physics-based engine model, built using the well-known mean-value engine modeling (MVEM) technique [22]–[24]. The model is verified in steady-state as well as during transients with the data obtained from the engine testbed. The use of such physics-based model allows to evaluate the effect of the parameter variation on the outputs of interest and tune the controllers accordingly.

TABLE I
ENGINE TESTBED CHARACTERISTICS

Type	Turbocharged common rail diesel engine
General data	In-line 4 cylinders, 4-stroke, 4.4 L
Power	115 kW @ 2200 rpm
Torque	600 Nm @ 1400 rpm
Turbocharger	VGT
EGR	No
Dynamometer	Electromagnetic
Control interface	NI LabVIEW full engine control

Any variation of the process parameters implies the possibility of controller going unstable. Therefore, the robustness and stability of the control system have to be evaluated before deploying the controller to the engine testbed. It is clear that to prove these analytically for the nonlinear system regulated in closed-loop with the linear time-varying (LTV) adaptive controller is a non-trivial task. Therefore, the robustness and stability of the designed controller is confirmed via simulations with the full-order nonlinear model.

Finally, the adaptive controller is verified on the engine testbed in a series of experiments. Rapid prototyping of the controller is done in Labview while the controller itself is implemented in Simulink. The robustness to the variation of the actuator dynamics is assessed for the adaptive and fixed-parameter PI-controllers where the latter serves as a baseline controller for comparison.

The remainder of the paper is structured as follows. In Section II the engine configuration alongside with its physics-based model is presented and the validation is done with the measured data. Section III presents the design procedure of the adaptive control system, including the model linearization and control algorithm implementation. The stability of the control system under nominal dynamics is also discussed. The adaptive control system is tuned and its performance, stability and robustness is evaluated numerically in Section IV. Finally, in Section V the adaptive controller is validated with on-engine tests and its performance is compared to the fixed-parameter control approach (PI-controller). The work is concluded in Section VI.

II. ENGINE DESCRIPTION AND MODELING

The engine testbed used for evaluating the designed controller consists of 4.4 liter 4-cylinders CI diesel engine linked to electromagnetic dynamometer. The variable geometry turbocharger is installed to regulate the boost pressure. Exhaust gas recirculation is not present in this engine layout. The testbed characteristics are summarized in Table I. The block diagram demonstrating closed-loop boost pressure control configuration is shown in Fig. 1.

The boost pressure set-point $p_i^{\mathrm{sp}} = f(\omega_e, M_e)$ is taken from the engine map and depends on the current engine operating point described by rotational speed ω_e and

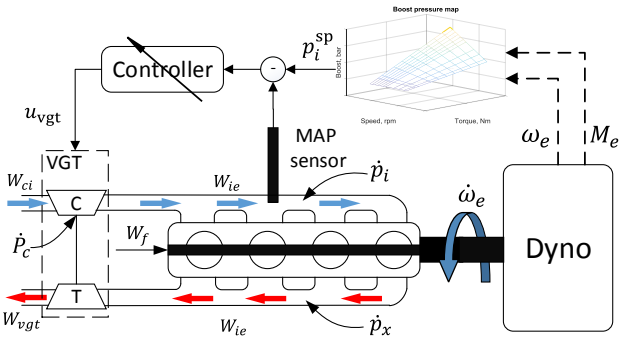

Fig. 1. Block-diagram of the closed-loop boost pressure control for CI engine. Boost pressure set-point is taken from the optimal map $p_i^{\text{sp}} = f(\omega_e, M_e)$. The mass flows used in modeling are denoted W_{xx}. C stands for the compressor, T for the variable geometry turbine. The states of the model air- ($\dot{p}_i$, $\dot{p}_x$, $\dot{P}_c$) and fuel-path ($\dot{\omega}_e$) are also marked.

load M_e. In this work, the map is taken as is from the manufacturer. Initially, the control tuning is done by means of numerical simulation in order to save the testbed operating time. Thus, a reliable control-oriented model of the engine needs to be constructed. The physics-based modeling approach is preferred as it allows to evaluate the effect of parameter variation on process dynamics in a realistic way as compared to the black-box identified models. In addition, the model will allow to assess the controller adaptation to the parameter variation which is hard to perform directly on the testbed without prior simulation.

A. First-principles model

The fourth-order physics-based model of the engine is developed using the standard mean-value modeling technique (interested reader is referred to [22]–[24] for more details on MVEM). Such model has been shown to accurately represent the main engine dynamics which is important for the realistic simulation and control system testing before deploying it to the actual engine testbed.

The model consists of 3 states (intake p_i and exhaust p_x pressure and the compressor power P_c) describing the engine air-path (as suggested in [25]) and one state (engine rotational speed ω_e) describing the fuel-path and is shown in Eq. 1. The air- and fuel-path sub-models are described below.

1) Air-path sub-model: the mass flows are denoted as W_{xx} and are shown in Eq. 2, where the subscript xx can be ci (compressor→intake), ie (intake→exhaust), vgt (turbocharger), f (fuel). The time-dependency (t) in the model equations is omitted for simplicity. The flow correction coefficient $\psi(\cdot)$ is defined in [23].

The dynamics of the VGT are described by the power transfer between the turbine and compressor with time constant τ_c as proposed in [25]. The power of the turbine P_{vgt} is defined as

$$P_{\text{vgt}} = \eta_{\text{t}} W_{\text{vgt}} c_p T_x \left(1 - \left(\frac{p_a}{p_x}\right)^{\mu_x}\right) \tag{3}$$

$$\begin{aligned}
\dot{p}_i &= \frac{R_i T_i}{V_i}(W_{ci} - W_{ie}) \\
\dot{p}_x &= \frac{R_x T_x}{V_x}(W_{ie} + W_f - W_{vgt}) \\
\dot{P}_c &= \frac{1}{\tau_c}(P_{\text{vgt}} - P_c) \\
\dot{\omega}_e &= \frac{1}{J}(M_e - M_l)
\end{aligned} \tag{1}$$

$$\begin{aligned}
W_{ci} &= \frac{\eta_c P_c}{T_a c_{p,i}\left(\left(\frac{p_i}{p_a}\right)^{\mu_c} - 1\right)} \\
W_{ie} &= \frac{V_d \omega_e p_i}{v 2\pi R_i T_i}\eta_v(\omega_e, p_i, \ldots) \\
W_{vgt} &= A_{vgt} f(u^*_{vgt}) \frac{p_x}{\sqrt{R_x T_x}} \psi_t(p_{r,t})
\end{aligned} \tag{2}$$

where the turbine efficiency is defined as η_{t}.

The turbine η_t and compressor η_c efficiencies as well as intake T_i and exhaust T_x temperatures are kept constant during numerical simulations. This is obviously a crude approximation and the above mentioned parameters vary at different engine operating conditions. However, such approximation has been shown to catch the relevant engine dynamics within the narrow range of speeds investigated in this work.

2) Fuel-path sub-model: the engine torque M_{e} is inversely proportional to engine speed ω_e and also depends on the amount of injected fuel W_f and indicated engine efficiency η_i

$$M_{\text{e}} = \frac{W_f H_i}{\omega_e}\eta_i(\omega_e, \lambda) \tag{4}$$

where H_i is the lower heating value of the fuel, the indicated efficiency is defined as $\eta_i(\omega_e, \lambda) = (a_1 + a_2\omega_e + a_3\omega_e^2)(1 - a_4\lambda^{a_5})$ and λ is the normalized air-fuel ratio [22]. Also, the engine volumetric efficiency is taken from [22] as the second-order speed-polynomial $\eta_v = a_{v1} + a_{v2}\omega_e + a_{v3}\omega_e^2$, where $a_1 \ldots a_5$ as well as $a_{v1} \ldots a_{v3}$ are the tuning parameters.

In this work, standard PI controller is used for closed-loop control of engine rotational speed ω_e (which is measured), where the fuel mass flow W_f is regarded as control input in numerical simulations (i.e. W_f is the output of the PI controller).

Dynamics that are the most relevant for this work from the control point of view are the intake manifold (or boost) pressure $p_i(t)$ and the engine speed $\omega_e(t)$. These two together are capable of describing the engine operation sufficiently well for the control design and at the same time providing a room for physics-based analysis of dynamics variation.

3) Control goal: the main goal of this work is to regulate the intake manifold pressure p_i to the desired set-point p_i^{sp} by changing guide vanes of the VGT with

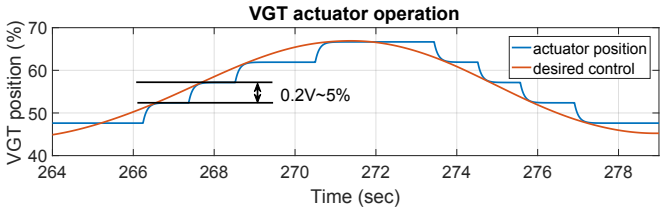

Fig. 2. Operating principle of the VGT guide vanes actuator. The desired position is generated by the boost pressure controller. The actuator position is limited by the discretization step of 0.2 V ($\sim 5\%$)

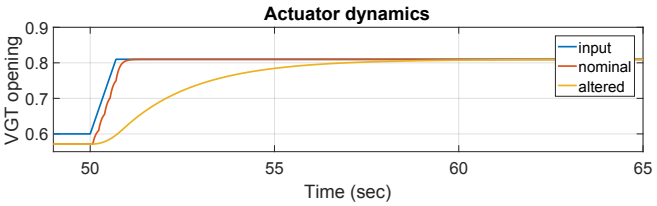

Fig. 3. Dynamics of the VGT actuator. Commanded input is shown together with the actual actuator position. The degraded actuator is represented with the process $G_{\text{act}}^{\text{total}}$.

the control signal u_{vgt} in spite of the engine dynamics variation when the engine is run at constant speed subject to load disturbance (marine application operating scenario).

B. Actuator modeling

1) Nominal dynamics: the actuator used to drive the guide vanes of the VGT is modeled in this section. The full operating range of VGT actuation from closed (0%) to open (100%) corresponds to 0 and 4.2 V, respectively. However, this particular actuator can only operate at discrete time instances with the increment of $\delta_{\text{act}} = 0.2$ V within that range as shown in Fig. 2. Thus, there is a limited amount of positions u_{act} the actuator can take, and it remains static unless the desired control signal exceeds the nearest mechanically possible actuator position. Therefore, the actual position of the actuator is always delayed after the desired control signal.

We point out that while this kind of actuation prevents the excessive movement of the actuator and reduces mechanical wear, the downside is the inability of the controller to settle down if the desired VGT position (generated by controller) happens to be in between the physically possible ones (which is often the case). This creates additional difficulty for the control system, introducing a sort of an actuator stiction.

The nominal dynamics of the actuator can be described by the following first-order transfer function

$$G_{\text{act}}(s) = \frac{u^*_{\text{vgt}}}{u_{\text{vgt}}} = \frac{1}{\tau_{\text{act}} s + 1} \tag{5}$$

with the nominal time-constant τ_{act}. The control signal generated by the controller is denoted as u_{vgt} and the actual control affecting the system is u^*_{vgt}.

2) Altered dynamics: the dynamics variation dealt with in this work is assumed to affect the actuator via altering its nominal transfer function in the following way

$$G_{\text{act}}^{\text{total}}(s) = G_{act}(s) \frac{1}{\delta\tau_{\text{act,max}} s + 1} \tag{6}$$

where the time constant is chosen as $\delta\tau_{\text{act,max}} = 2$ sec. The comparison of the original and degraded response of the VGT actuator is shown in Fig. 3.

C. Model validation with experimental data

The physics-based air and fuel-path model has been validated with the measured data from the engine testbed. In order to be used for the control design, the model has to provide reasonable match for the dynamics of interest (e.g., speed and boost pressure) during transients and also in steady-state. The values for the physical engine parameters, including dimensions (e.g., manifold volumes, bore, stroke, etc.) and thermodynamic parameters (e.g., specific gas constants, heat ratios) are known. Thus, the tuning parameters $a_1 \dots a_5$ as well as $a_{v1} \dots a_{v3}$ are used to fit the experimental data.

The engine on-board cargo vessels operates presumably at constant rotational speed disturbed by the load transients [7]. Thus, the model parameter estimation and validation is done in the operating region around the chosen engine speed of $1200 \dots 1600$ rpm and load range of $100 \dots 300$ Nm with transients of 50 Nm. Both estimation and validation is done with the engine speed controlled in a closed-loop with PI controller. The boost pressure p_i is controlled in an open-loop for estimation and in a closed-loop for validation and is discussed below.

1) Estimation: the unknown parameters are estimated using the Matlab parameter estimation toolbox. The estimation data together with the model prediction for speed 1400 rpm and load transients is demonstrated in Fig. 4. The achieved match is considered sufficient for the control design purposes as the transient response and the speed-load interaction are captured well.

The experimental data in Fig. 4 demonstrated insignificant speed fluctuations in steady-state which resulted from the interaction with the control-loop not considered in the simple model used here (i.e. common rail fuel pressure control). In addition, experimental data shows that the speed fluctuations at high load are stronger than those at lower load. These stem from the nonlinearities related to the CR fuel injection system which is not modeled here and, therefore, are not caught well in the present model (where disturbances in speed are of the same amplitude at various loads).

Figure 5 shows the data match for the measured and modeled response of the boost pressure when the turbocharger is controlled in an open-loop, and speed and load are constant. The non-linearity of the boost pressure can be clearly seen as the effect of the turbocharger gets

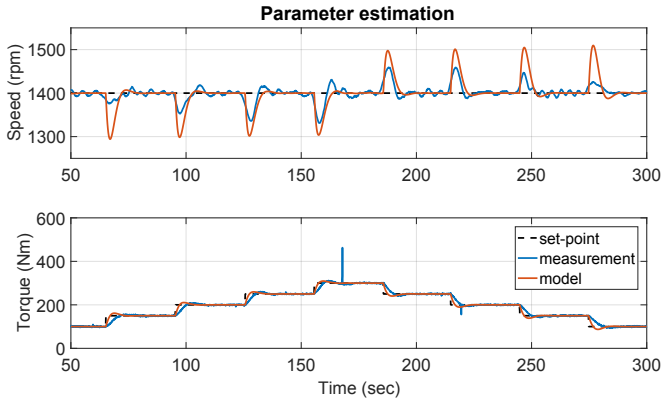

Fig. 4. Parameter estimation data. Measured and modeled data is plotted for constant speed $\omega_e = 1400$ rpm (top) and load transients M_e (bottom) of 50 Nm in the range of $100 \ldots 300$ Nm.

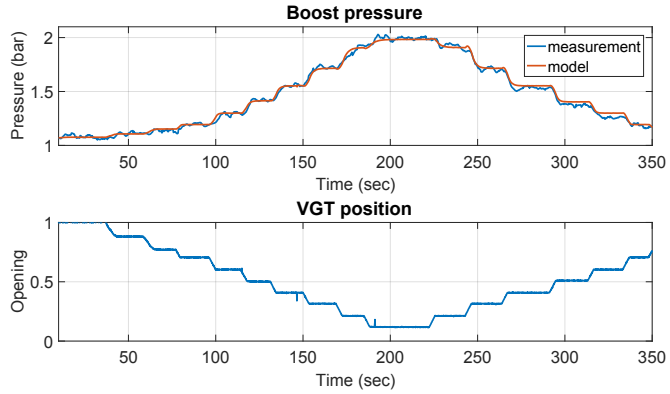

Fig. 5. Parameter estimation data. Open-loop measured and modeled boost pressure comparison at $\omega_e = 1400$ rpm and $M_e = 200$ Nm (top). VGT actuator position u^*_{vgt} is also shown (bottom).

higher with smaller openings. The parabolic function of the form

$$f(u^*_{\text{vgt}}) = 0.22 + 0.43u^*_{\text{vgt}} + 0.37(u^*_{\text{vgt}})^2 \qquad (7)$$

was fitted to obtain good steady-state data fit for the modeled boost pressure. It can be seen in Eq. 2 that the function $f(u^*_{\text{vgt}})$ affects how the control signal u^*_{vgt} alters the effective area A_{vgt} of the VGT and thereby the mass flow W_{vgt} through it.

The function is plotted in Fig. 6 against the desired VGT control signal and it can be clearly seen that most of the curvature appears at low openings while the VGT behavior is almost linear at larger openings.

2) Validation: in order to validate the model, another set of data has been recorded at two different speed set-points of 1200 and 1600 rpm and same load transients. Figure 7 shows that the match between the model and the experimental data is similar to the one obtained during estimation in Fig. 4.

In addition, the validation data for the boost-pressure is shown in Fig. 8. In this figure, the boost-pressure was controlled in a closed-loop using a PI-controller while the engine was operated at constant speed and load

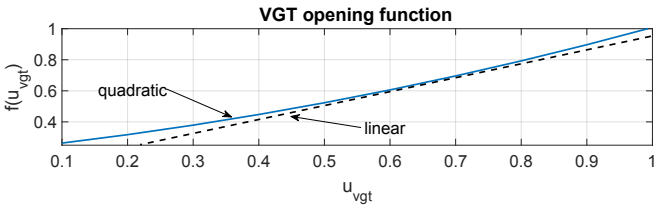

Fig. 6. Quadratic function fitted for VGT opening to obtain a good match between modeled p_i^{model} and measured p_i^{meas} boost pressure. The behavior of the VGT opening is almost linear at large openings while most of the curvature is in the low u_{vgt} range. The dashed line denotes linear function of u_{vgt} for comparison.

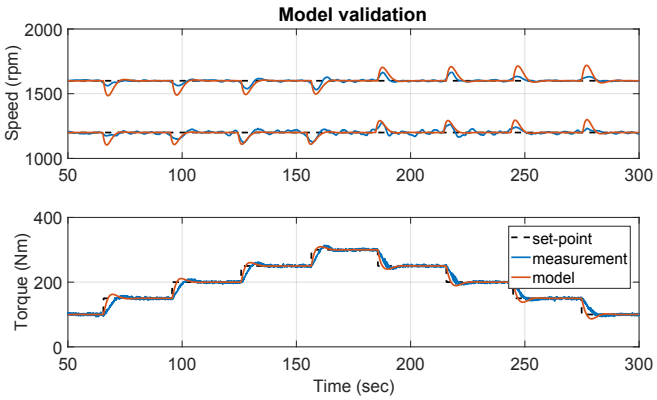

Fig. 7. Model validation data. Measured and modeled data is plotted for constant speed $\omega_e = 1200$ and $\omega_e = 1600$ rpm (top) and load transients M_e (bottom) of 50 Nm in the range of $100 \ldots 300$ Nm.

transients. The boost-pressure set-point p_i^{sp} was taken from the engine control map $f(\omega_e, M_e)$. Note that, the set-point p_i^{sp} appear to vary like a dynamic variable because it is a function of the engine speed ω_e.

Figure 8 shows that the match between measured and modeled boost pressure p_i as well as between the control signals (i.e. real and modeled VGT actuator position) is satisfactory.

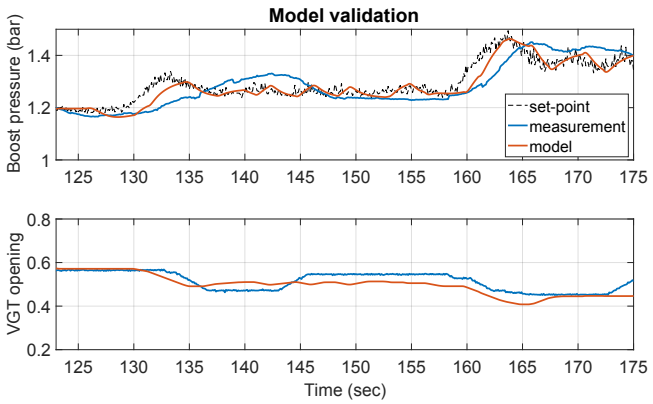

Fig. 8. Model validation. Measured and modeled data is plotted for the boost pressure p_i (corresponds to the OP shown in Fig. 4). VGT actuator position u^*_{vgt} is also shown (bottom).

III. Control design

This section presents the control design procedure of the indirect adaptive controller. The analysis of the designed adaptive control system (process-observer-controller) is done using the linear time-invariant (LTI) approximation of the physics-based model (Eq. 1-7). The stability property of the indirect adaptive control algorithm is briefly discussed based on the linear approximation of the process.

A. Linearization

The model linearization is done using the Taylor series expansion. In order to perform the linearization, we first represent the physics-based model from Eq. 1-7 as nonlinear state-space equations

$$\dot{\mathbf{x}}(t) = \mathbf{f}(\mathbf{x}(\mathbf{t}), u(t)) + q \tag{8a}$$
$$z(t) = x_1(t) + r \tag{8b}$$

where z is the controlled output and the process and measurement noises are defined as $q \sim N(0, Q_1)$ and $r \sim N(0, Q_2)$, respectively. The vectors of the states as well as the process input and output are defined as

$$\begin{aligned} \boldsymbol{x} &= \big[\underbrace{p_i \quad p_x \quad P_c}_{\text{air-path}} \;\big|\; \underbrace{\omega_e}_{\text{fuel-path}}\big]^T, \rightarrow \text{combined states} \\ u &= u_{\text{vgt}} \rightarrow \text{control input} \\ z &= p_i \rightarrow \text{measured output}, \end{aligned} \tag{9}$$

respectively.

The linearized matrices $\mathbf{A}(t)$ and $\mathbf{B}(t)$ represent the Jacobians of the nonlinear state function $\mathbf{f}(\mathbf{x}(\mathbf{t}), \mathbf{u}(\mathbf{t}))$ with respect to states and inputs

$$\mathbf{A}(t) = \left.\frac{\partial \mathbf{f}}{\partial \mathbf{x}}\right|_{\mathbf{x}_{\text{lp}}, u_{\text{vgt,lp}}} \qquad \mathbf{B}(t) = \left.\frac{\partial \mathbf{f}}{\partial u}\right|_{\mathbf{x}_{\text{lp}}, u_{\text{vgt,lp}}} \tag{10}$$

where $\mathbf{x}_{\text{lp}}$ and $u_{\text{vgt,lp}}$ define the linearization point (LP). The controlled output is the intake manifold pressure p_i, and the output $\mathbf{C}$ matrix is therefore formed as

$$\mathbf{C} = \begin{bmatrix} 1 & 0 & 0 & 0 \end{bmatrix}. \tag{11}$$

The linear-time varying state-space model can now be written

$$\begin{aligned} \dot{\mathbf{x}}_{4\times 1} &= \mathbf{A}(t)\mathbf{x}_{4\times 1} + \mathbf{B}(t)u \\ \mathbf{z} &= \mathbf{C}\mathbf{x}_{4\times 1}. \end{aligned} \tag{12}$$

where $\mathbf{A}(t) \in \mathbb{R}^{4\times 4}$ and $\mathbf{B}(t) \in \mathbb{R}^{4\times 1}$. However, a linear time-invariant transfer function is required for the adaptive control design. It can be derived via using the well-known equality $\mathbf{G}(s) = \mathbf{C}(s\mathbf{I} - \mathbf{A})^{-1}\mathbf{B}$ and fixing the obtained matrices $\mathbf{A}$ and $\mathbf{B}$ at each point defined by the VGT opening u_{vgt}.

The order of the obtained 4^{th} system is reduced via using the balanced order reduction method. The goal is to reduce the order in such a way that the response of the model is preserved over the low frequency range of interest. In our case a second order approximation of the full order model has been found to be accurate and will be therefore used for control design and analysis.

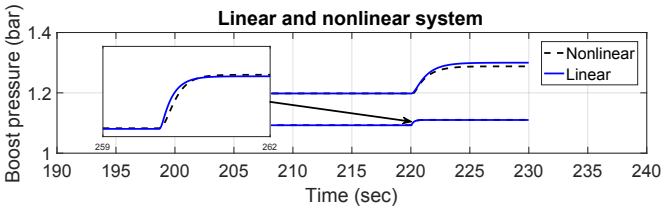

Fig. 9. Comparison of the step response of the linear and nonlinear model at two linearization points is demonstrated (VGT). The larger step corresponds to VGT position $60 \rightarrow 50\%$ and smaller $100 \rightarrow 90\%$. The linear model is stable and minimum-phase within the engine operating range.

The resultant transfer function at each LP is defined as

$$G(s)|_{u_{\text{vgt}}} = k\frac{s - z_1}{(s - p_1)(s - p_2)}. \tag{13}$$

In order to validate that the nonlinear model is represented well by its linear approximation, the step responses of both are compared. Figure 9 demonstrates the steps done at two different VGT positions of $60 \rightarrow 50\%$ and $100 \rightarrow 90\%$ which correspond to different levels of intake manifold pressure. It can be seen that the linear model has a slight offset at higher pressure level, although the transient is similar. Also, the reverse control action of $u_{\text{vgt}} \rightarrow p_i$ (i.e. the increase in the control signal u_{vgt} causes the boost pressure p_i to decrease) is well captured. It can be seen that the process is stable and of minimum phase. As it is important for the plant to possess the property of the minimum-phase (from u_{vgt} to p_i) for the indirect MRAC design, an additional set of experiments has been done on the engine testbed. Figure 10 demonstrates the steps in VGT position with the amplitude of about 25% (closing) and 50% (opening) as well as the boost pressure p_i response. These steps are performed at two different OPs in order to confirm the absence of the non-minimum phase property for the entire operating range dealt with in this work.

Therefore, for the rest of this work the plant $G(s)$ is assumed to be minimum-phase within the considered operating range.

B. Indirect model reference adaptive control

In this work, a variation of model reference adaptive control algorithm is proposed for dealing with the time-varying engine dynamics. Specifically, the indirect version of MRAC is utilized because it possesses guaranteed asymptotic stability property for our system under several assumptions which we review in the next subsection. In addition, indirect adaptive control offers flexibility concerning the identifier and the controller as these are represented by separate subsystems.

The idea of the indirect adaptive control algorithm is to first construct the fixed-parameter control structure

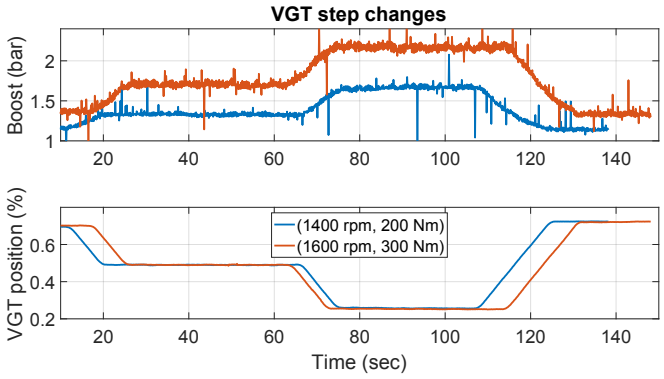

Fig. 10. Experimental data: the VGT step changes are done at two different OP (1400 rpm, 200 Nm) and (1600 rpm, 300 Nm). It can be seen that the response is minimum phase.

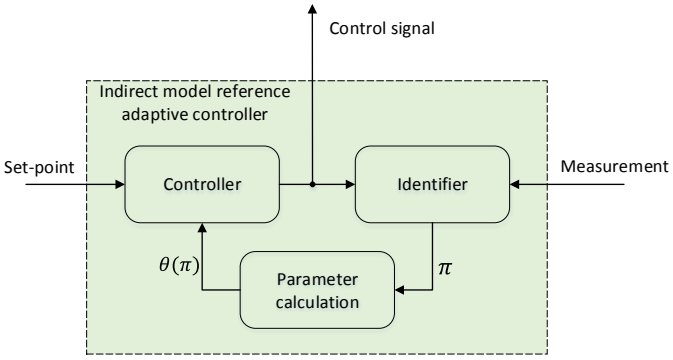

Fig. 11. Block-diagram of indirect model reference adaptive controller.

with parameters being functions of the plant parameters. These parameters are then replaced by their estimates obtained via recursive online identification, thus making the overall controller adaptive. While the indirect MRAC has been discussed in details in [13], [26], we review its implementation for our particular system hereafter. The indirect MRAC is demonstrated in Fig. 11 and consists of the controller, identifier and the parameter transformation block.

The indirect adaptive control scheme utilizes the identification (rather than tracking) error as the core of the update mechanism

$$e = p_i^{\text{ident}} - p_i \tag{14}$$

where p_i^{ident} and p_i are the identified and measured boost pressure, respectively. The desired behavior of the closed-loop system in model-reference control is determined by the linear model defined in such a way that its relative degree is the same as the degree of the process

$$M(s) = k_m \frac{n_m(s)}{d_m(s)} = \frac{\omega_m^2 s + 1}{s^2 + 2\zeta_m \omega_m s + \omega_m^2}, \tag{15}$$

where k_m, $n_m(s)$, $d_m(s)$ are the model gain, numerator and denominator polynomials, respectively, and ω_m and ζ_m are the tuning parameters that can be adjusted in order to obtain a desired response.

1) Observer: the goal of the observer is to produce a recursive estimate of the process parameters k, z_1, p_1 and p_2 which can then be used to construct a controller. In order to achieve this, a parametrization of the process in Eq. 13 is introduced in a way that these and identified parameters are related linearly

$$G(s) = \frac{p_i}{p_i^{\text{sp}}} = k_p \frac{n_p(s)}{d_p(s)} = \frac{\alpha_2 s + \alpha_1}{s^2 + \beta_2 s + \beta_1}, \tag{16}$$

where k_p, $n_p(s)$ and $d_p(s)$ denote the process gain, numerator and denominator polynomials, respectively. The following expression can be derived easily

$$s^2 p_i = (\alpha_2 s + \alpha_1) p_i^{\text{sp}} - (\beta_2 s + \beta_1) p_i. \tag{17}$$

As the derivatives of p_i and p_i^{sp} are not available, the Hurwitz polynomial $\xi(s) = s^2 + \xi_2 s + \xi_1$ is introduced to remedy this problem. Therefore, the parametrization of the output p_i can be written as

$$p_i = \frac{a(s)}{\xi(s)}(p_i^{\text{sp}}) + \frac{b(s)}{\xi(s)}(p_i) \tag{18}$$

where the time-varying polynomials $a(s)$ and $b(s)$ are defined as

$$\begin{aligned} a(s) &= \alpha_2 s + \alpha_1 = k_p n_p(s) \\ b(s) &= (\xi_2 - \beta_2)s + (\xi_1 - \beta_1) = \xi(s) - d_p(s) \end{aligned} \tag{19}$$

In order to proceed to recursive parameter identification and control, Eq. 18 needs to be converted to time-domain. This can be done by introducing the following notation

$$\boldsymbol{\Xi} = \begin{bmatrix} 0 & 1 \\ -\xi_1 & -\xi_2 \end{bmatrix} \quad \boldsymbol{b_\xi} = \begin{bmatrix} 0 \\ 1 \end{bmatrix} \tag{20}$$

and defining the filters $\dot{\boldsymbol{w}}^{(i)}$ for set-point p_i^{sp} and output p_i as

$$\begin{aligned} \dot{\boldsymbol{w}}^{(1)} &= \boldsymbol{\Xi} \boldsymbol{w}^{(1)} + \boldsymbol{b_\xi} p_i^{\text{sp}} \\ \dot{\boldsymbol{w}}^{(2)} &= \boldsymbol{\Xi} \boldsymbol{w}^{(2)} + \boldsymbol{b_\xi} p_i, \end{aligned} \tag{21}$$

The process output p_i from Eq. 18 can now be easily written in time-domain as

$$p_i(t) = a^{*T} \boldsymbol{w}^{(1)}(t) + b^{*T} \boldsymbol{w}^{(2)}(t) = \boldsymbol{\pi}^* \widetilde{\boldsymbol{w}} \tag{22}$$

where the parameter vector $\boldsymbol{\pi}^*$ (* denotes the nominal parameter value) is defined as

$$\boldsymbol{\pi}^* = \big[\underbrace{a_1^* \quad a_2^*}_{a^{*T}} \quad \underbrace{b_1^* \quad b_2^*}_{b^{*T}}\big] = \big[\alpha_1^* \quad \alpha_2^* \quad \xi_1 - \beta_1^* \quad \xi_2 - \beta_2^*\big] \tag{23}$$

and

$$\widetilde{\boldsymbol{w}} = \begin{bmatrix} w_1^{(1)} & w_2^{(1)} & w_1^{(2)} & w_2^{(2)} \end{bmatrix} \in \mathbb{R}^4 \tag{24}$$

The identified output of the process p_i^{ident} is written in a similar fashion to Eq. 22 as

$$p_i^{\text{ident}} = \boldsymbol{\pi} \widetilde{\boldsymbol{w}}^T \tag{25}$$

A gradient descent method is employed to recursively update the parameter vector $\boldsymbol{\pi}$ as the new measurements become available

$$\dot{\boldsymbol{\pi}} = -\gamma e \widetilde{\boldsymbol{w}}, \tag{26}$$

where $\gamma > 0$ is the tuning parameter which solely determines the parameter convergence speed.

The update law is extended with robustness modification similar to the ones discussed in [27], [28]

$$\dot{\boldsymbol{\pi}} = -\gamma e \widetilde{\boldsymbol{w}} - \sigma(\pi - \pi_0), \tag{27}$$

where $\boldsymbol{\pi}_0$ denotes the previous estimate of $\boldsymbol{\pi}$. Such a modification aims at preventing the unbounded growth of the parameter vector $\boldsymbol{\pi}$ and keeps the parameters close to their previous estimate $\boldsymbol{\pi}_0$.

2) Controller: the controller structure itself was proposed in [13] as

$$\begin{aligned} u_{\mathrm{vgt}} = c_0 p_i^{\mathrm{sp}} + \frac{c(s)}{\xi(s)} u_{\mathrm{vgt}} + \frac{d(s)}{\xi(s)} p_i \rightarrow \\ \rightarrow u_{\mathrm{vgt}} = \frac{\xi(s)}{\xi(s) - c(s)} (c_0 p_i^{\mathrm{sp}} + \frac{d(s)}{\xi(s)} p_i) \end{aligned} \tag{28}$$

where $c(s)$ and $d(s)$ are the time-varying controller polynomials. Combining the latter with

$$p_i = k_p \frac{n_p(s)}{d_p(s)} u_{\mathrm{vgt}} \tag{29}$$

we can write the transfer function from $p_i^{\mathrm{sp}} \rightarrow p_i$

$$\frac{p_i}{p_i^{\mathrm{sp}}} = \frac{c_0 k_p \xi(s) n_p(s)}{(\xi(s) - c(s)) d_p(s) - k_p n_p(s) d(s)} \tag{30}$$

Since the goal of the controller is the model following, the foregoing transfer function has to match the model $M(s)$ defined in Eq. 15. Therefore, by defining $\xi(s) = \xi_0(s) n_m(s)$, we can easily write the matching equality $M(s) \leftrightarrow G(s)$ in order to evaluate the controller parameters $\boldsymbol{c}$ and $\boldsymbol{d}$

$$\begin{aligned} (\xi_0(s) n_m(s) - c(s)) d_p(s) - k_p(s) n_p(s) d(s) = \\ c_0 \frac{k_p}{k_m} \xi_0(s) d_m(s) n_p(s) \end{aligned} \tag{31}$$

Recalling the parametrization in Eq. 19 the time-varying controller polynomials become apparent

$$\begin{aligned} c(s) &= \xi(s) - \frac{1}{a_2} q(s) a(s) \\ d(s) &= \frac{1}{a_2} (q(s)\xi(s) - q(s) b(s) - \xi_0 d_m(s)) \\ c_0 &= \frac{k_m}{a_2}, \end{aligned} \tag{32}$$

where $a(s)$ and $b(s)$ are polynomials defined in Eq. 19, and the quotient $q(s)$ is evaluated as

$$q(s) = \frac{\xi_0(s) d_m(s)}{\xi(s) - b(s)} \tag{33}$$

The proposed adaptive controller in Eq. 28 does not include the knowledge on the saturation limits of the generated control signal naturally and these must therefore be physically enforced

$$\begin{cases} u_{\mathrm{vgt}} = 0 & \text{if} \quad u_{\mathrm{vgt}} \leq 0 \\ u_{\mathrm{vgt}} = \boldsymbol{\theta} \boldsymbol{w}^T & \text{if} \quad 0 < u_{\mathrm{vgt}} < 1 \\ u_{\mathrm{vgt}} = 1 & \text{if} \quad u_{\mathrm{vgt}} \geq 1 \end{cases} \tag{34}$$

where 0 corresponds to fully closed VGT, 1 to fully open and the vectors are

$$\boldsymbol{\theta} = \begin{bmatrix} c_0 & c_1 & c_2 & d_1 & d_2 \end{bmatrix} \in \mathbb{R}^5 \tag{35a}$$

$$\boldsymbol{w} = \begin{bmatrix} p_i^{\mathrm{sp}} & \boldsymbol{w}^{(1)^T} & \boldsymbol{w}^{(2)^T} \end{bmatrix} \in \mathbb{R}^5 \tag{35b}$$

where c_0, c_1, c_2, d_1 and d_2 are the coefficients of time-varying polynomials defined in Eq. 32.

C. Stability

The diesel engine model in Section II-A represents a set of nonlinear coupled ODEs (Eq. 1-4). The closed-loop control of such a system with adaptive LTV controller makes analytical stability proof a nontrivial task. Therefore, in this section, we consider stability of the indirect MRAC via a local linear approximation $G(s)$ (Eq. 13) of the original process model, and the stability of the full nonlinear adaptive control system will be demonstrated by means of simulation and experiments in Sections IV and V, respectively.

When it comes to model reference adaptive control, the stability can not be proved using the Lyapunov approach as it requires the assumption on the parameters to be initially sufficiently close to their nominal (optimal) values. In MRAC there is typically no knowledge of the true parameter values. Therefore, the concept of bounded-input bounded-state (BIBS) stability is normally used.

The proposed indirect MRAC system has been proved (see Theorem 3.7.3 from [13]) to be BIBS stable (that is for any p_i^{sp} bounded, and $\mathbf{x}(\mathbf{0}) \in \mathbb{R}^{10}$ (combined state of the model, observer and controller), the solution $\mathbf{x}(\mathbf{t})$ remains bounded) under the following assumptions:

1) The process has to be SISO linear-time invariant (LTI) strictly proper minimum phase system defined in accordance with $G(s) = k_p n_p(s)/d_p(s)$ with lower-bounded high-frequency gain k_p. These criteria are satisfied by the transfer function $G(s)$ of the linearized process defined in Eq. 13.
   Note: in this work, however, a major interest is to evaluate the ability of the controller to adapt to time-varying dynamics of the engine. It is known, that the mechanical wear and tear is typically a long term process and the dynamics are therefore slowly-time varying. By the definition, such system can be considered to be LTI on a small scale (i.e. approximately invariant during a short period of time) thus satisfying the stability assumption. The key point here is that the adaptation should always occur faster than the parameter variation, to provide the parameter $\pi \rightarrow \pi^*$ convergence, where π^* is the nominal parameter value. Therefore, the aggressiveness of the process identification γ in Eq. 26 should be chosen to satisfy the fast adaptation requirement, which can typically be done by trial and error method.
2) The stable, minimum phase model has to be defined in accordance with $M(s) = k_m n_m(s)/d_m(s)$

TABLE II
PARAMETERS OF THE INDIRECT MRAC

Controller gain γ	1
Sigma modification gain σ	0.1
Model $M(s)$ natural frequency ω	1
Model $M(s)$ damping coefficient ζ	1
Identifier parameter $\boldsymbol{\Xi}$	$\begin{bmatrix} 0 & 1 \\ -1 & -2 \end{bmatrix}$
Identifier parameter $\boldsymbol{b_\xi}$	$\begin{bmatrix} 0 & 1 \end{bmatrix}^T$
Initial conditions for the parameters $\boldsymbol{\pi_0}$	$\begin{bmatrix} 0 & -1 & -5 & 0 \end{bmatrix}^T$

TABLE III
PARAMETERS OF THE PI CONTROLLER

Proportional gain P	0.3
Integral gain I	0.5

where monic polynomials $n_m(s)$ and $d_m(s)$ are of the same degree as corresponding plant polynomials and $k_m > 0$. The model in $M(s) = \frac{\omega_m^2 s+1}{s^2+2\zeta_m\omega_m s+\omega_m^2}$ in Eq. 15 is chosen accordingly, to provide the desired closed-loop performance.

3) The set-point p_i^{sp} utilized for the closed-loop boost pressure control is piecewise continuous and bounded on $\mathbb{R}_+$.

Thus, the proposed adaptive control system is BIBS stable (with the locally linearized engine model).

IV. SIMULATION RESULTS

Before the proposed adaptive control system is deployed to the engine testbed, its performance has been assessed via simulations in Matlab/Simulink. The engine mean value model defined in Eq. 1-7 has been used in simulations in place of the real engine. Not only this allows to assess the controller capabilities for set-point tracking (both in transient and steady-state operation) and adaptation to time-varying dynamics of the engine, but also to evaluate the stability and robustness of the controller numerically under different operating conditions.

The proposed controller has been tuned to achieve the desired step response by adjusting the gain γ, σ, model parameters ω, ζ, identifier parameters $\boldsymbol{\Xi}$, $\boldsymbol{b_\xi}$ and also the parameter initial conditions $\boldsymbol{\pi_0}$. The chosen parameters are listed in Table II. The initial conditions of the identifier parameters π_0 affect the step-response characteristics of the closed-loop system and their choice is essentially a trial-and-error process.

Figure 12 (top) shows the transient boost pressure set-point $p_i^{\text{sp}} = 1.2 \rightarrow 1.4$ bar tracking using MRAC at constant engine speed $\omega_e = 1500$ rpm and torque $M_e = 200$ Nm.

In this simulation, the engine operates with nominal (or initial tuning) dynamics defined in Eq. 5 until t=450 sec, when the VGT actuator behavior gets altered as in Eq. 6. For comparison, the response of the standard fixed-parameter PI-controller is also shown in the same

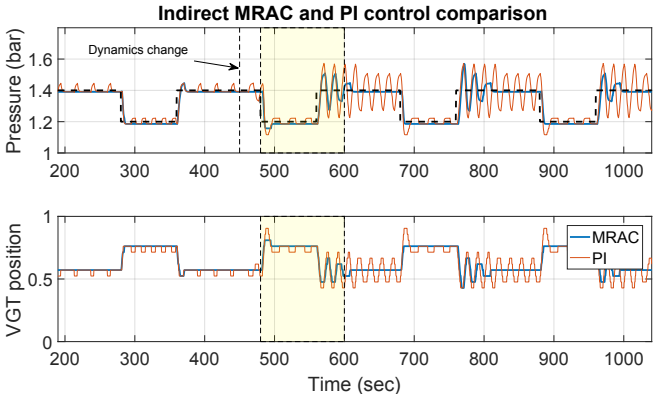

Fig. 12. Simulation results: transient boost pressure set-point ($p_i^{\text{sp}} = 1.2 \rightarrow 1.4$ bar) tracking with MRAC vs PID under nominal and altered dynamics of the VGT actuator. The time instant $t = 450$ s for dynamics change is marked with vertical dashed line.

Figure 12. The PI-controller was tuned to obtain the same rise time for the case of nominal actuator dynamics and its parameters are shown in Table III.

It can be seen that the PI-controlled engine demonstrates oscillatory response with the altered actuator dynamics when the boost pressure set-point is changed (at time $t = 490s$).

While the PI-controller keeps oscillating, the MRAC starts the adaptation once the new information (i.e. the change of the measured output) becomes available. The adaptation period is highlighted in yellow in Fig. 12 and it can be seen that some oscillations appear. The step response of the adapted controller has two overshoots, however settles down quickly.

It is worth noting here, that the actuator dynamics change in real-life scenario is a slowly-time varying process, i.e. slow parameter drift over extended period of time. However, the simulation was done with more aggressive dynamics variation in step-like fashion, for improved confidence and compactness of the data representation in Fig. 12. The actual position of the VGT actuator is also shown in Fig. 12 (bottom). As discussed in Section II-B the actual position cannot always match the desired one due to the limitations of the actuator. This causes a small steady state-offset for the boost pressure and control signal spikes (for example at $t = 220s$, $t = 240s$, $t = 260s$ for PID in Fig. 12 (top)).

The identifier parameters $\boldsymbol{\pi}$ of MRAC are shown in Fig. 13 (corresponds to the simulation in Fig. 12). It can be seen that the identifier parameters vary depending on the measured process output (e.g. t=250. . .450 s). The parameters update due to the altered engine dynamics is highlighted in yellow.

The corresponding control gains $\boldsymbol{\theta}$ are evaluated as discussed in Section III and are also shown in Fig. 13.

V. EXPERIMENTAL RESULTS

The engine testbed used for the adaptive control concept testing is shown in Fig. 14. The full engine control system (including closed-loop PI control for speed,

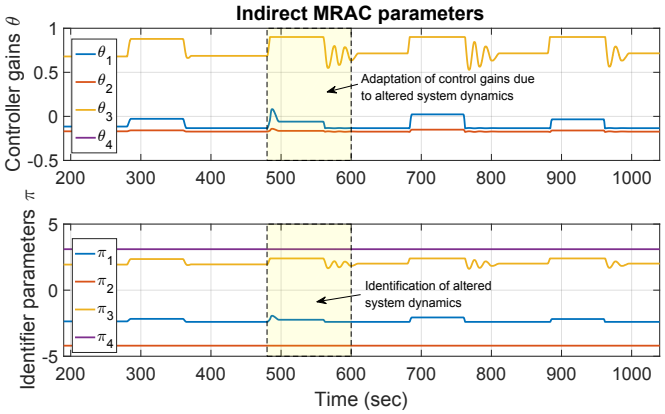

Fig. 13. Simulation results: parameter $\boldsymbol{\pi}$ identification of altered system dynamics with MRAC identifier as well as control gains $\boldsymbol{\theta}$ adaptation is shown. The regions of identification and gains' adaptation are highlighted in yellow.

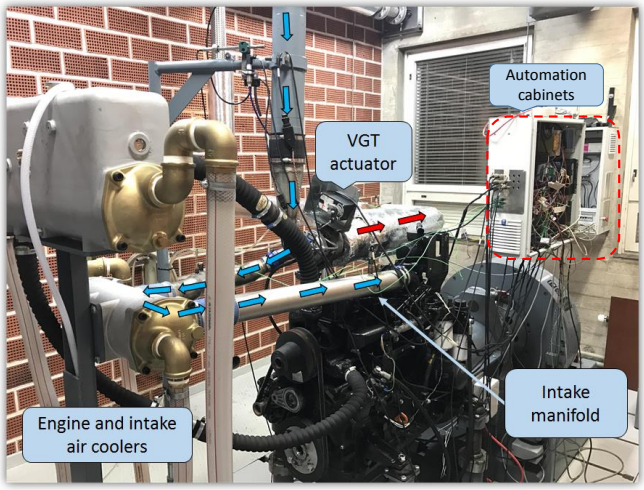

Fig. 14. Engine testbed on which all experiments discussed in this work have been performed. The air flow inside the engine is shown with arrows.

load, fuel pressure, etc.) is implemented using National Instruments (NI) rapid-prototyping hardware. The PI controllers are tuned manually and, therefore, no production type controllers is used. The proposed adaptive boost controller is constructed in Matlab/Simulink. It is then compiled into *.dll file in order to allow for the LabVIEW/Simulink co-simulation. All the measured data presented in this section was post-processed by applying a low-pass filter in order to eliminate the high-frequency measurement noise components and improve visual comprehension. The goal of this section is to confirm the results obtained via simulation.

Table IV summarizes the two verification test scenarios that have been set up for testing the adaptive controller. These test scenarios have been designed to evaluate the controllers ability to track sudden set-points variations as well as their ability to operate in real-world conditions when the engine operation at constant speed is affected by the load disturbance. The latter is the most popular

TABLE IV
EXPERIMENTAL VERIFICATION SCENARIOS FOR ADAPTIVE CONTROLLER

Scenario	Engine speed ω_e	Load M_l	Boost pressure set-point p_i^{sp}
1 (Evaluation)	Constant	Constant	Step
2 (Realistic)	Constant	Step	Optimal map

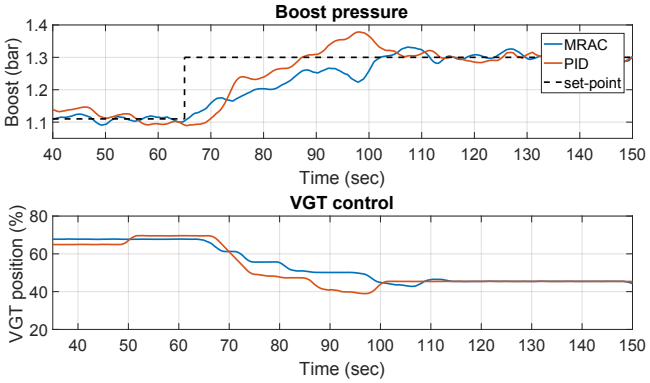

Fig. 15. Experimental results (evaluation): MRAC vs PID with nominal dynamics of the VGT actuator. The response of both controllers is demonstrated for step change in the boost pressure set-point $p_i^{sp} = 1.1 \rightarrow 1.3$ bar. The experiment is run at the engine speed $\omega_e = 1400$ rpm and load torque $M_e = 200$ Nm.

operating scenario in marine industry, especially when speaking about large cargo vessels.

The designed adaptive controller was deployed to the engine after being tuned in simulation as discussed in Section IV and little extra tuning was required to achieve better response for the real engine.

Both of the above scenarios have been evaluated with nominal and altered actuator dynamics. The altered dynamics conditions are implemented as software (rather than real actuator damage) in accordance with Section II-B. Such implementation allows for repeatable experiments without the need to replace the damaged components.

The fixed-parameter PI-controller is also evaluated in all of the test runs and serves as a baseline controller.

1) Test case 1: at first, both controllers are evaluated with nominal dynamics of the VGT actuator. Figure 15 demonstrates the test run for the scenario 1 when the engine was run @(1400 rpm, 200 Nm) and the step-change for the boost pressure set-point was done as $p_i^{\text{sp}} = 1.1 \rightarrow 1.3$ bar. It can be seen that the controllers are tuned for approximately the same time-domain characteristics and both are stable.

In the next run, the dynamics of the actuator were altered as discussed in Section II-B in order to imitate the degraded (worn out) performance. The same engine OP was used in this test run as in the previous run with the nominal parameters. The response of both controllers for the step-change in set-point $p_i^{\text{sp}} = 1.1 \rightarrow 1.3$ bar is demonstrated in Fig. 16. It can be clearly seen that the adaptive controller outperforms the fixed-parameters

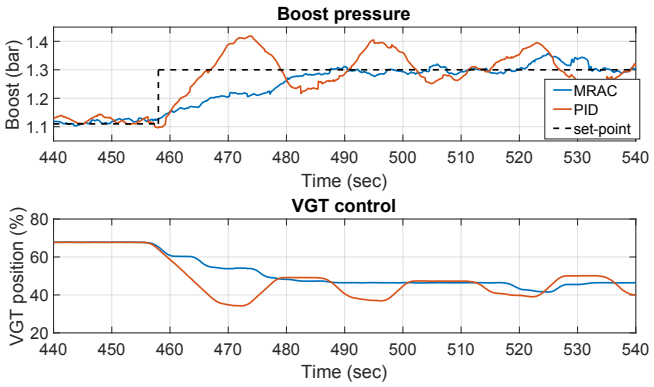

Fig. 16. Experimental results (evaluation): MRAC vs PID under altered dynamics of the VGT actuator. The response of both controllers is demonstrated for step change in the boost pressure set-point $p_i^{sp} = 1.1 \rightarrow 1.3$ bar. Considerable oscillations appear for PID-controlled engine. The experiment is run at the engine speed $\omega_e = 1400$ rpm and load torque $M_e = 200$ Nm.

PI-controller in the updated operating conditions. The time-domain characteristics of the engine response with MRAC remain relatively unaffected by the new actuator dynamics and the controller is stable. However, PI controller is strongly affected by the slower dynamics of the new actuator and becomes marginally stable.

2) Test case 2: once, the controllers have been validated at the steady-state engine OP, a more complicated test run was done using the realistic test-case scenario 2. In this scenario, the engine is still operated at constant speed of 1400 rpm, however this time the transient load is applied and the set-point for the boost pressure p_i^{sp} is taken from the reference map $f(\omega_e, M_e)$ (which again looks like a dynamic variable for reasons described in Subsection II-C). While the boost pressure set-point p_i^{sp} during load transient is similar to the manually chosen one (as in the previous test run), this experiment is more complicated for the boost controller. In this case, apart from actual set-point tracking, a load disturbance affecting the engine (and particularly boost pressure behavior) is added. Since this is the way, the engines are operated on-board ships, the controller have to be verified under such operating conditions. The recorded data for both adaptive and PI controllers is shown in Fig. 17 for the case of degraded actuator dynamics. It can be seen, that both controllers demonstrate performance similar to the previous run in Fig. 16. We note here that for the speed-load control of diesel engine the injected fuel quantity can typically be presented. However, in this work, the focus is done on boost pressure control and its adaptation and, therefore, the fueling data is omitted.

While the above-discussed oscillations of the boost pressure do not significantly degrade the engine rotational speed, they do affect the engine-out lambda. As lambda is known to be directly correlated to the engine emissions and smoke as well as the engine fuel consumption, it is highly undesirable to have lambda oscillating [29]. Figure 18 presents measured lambda

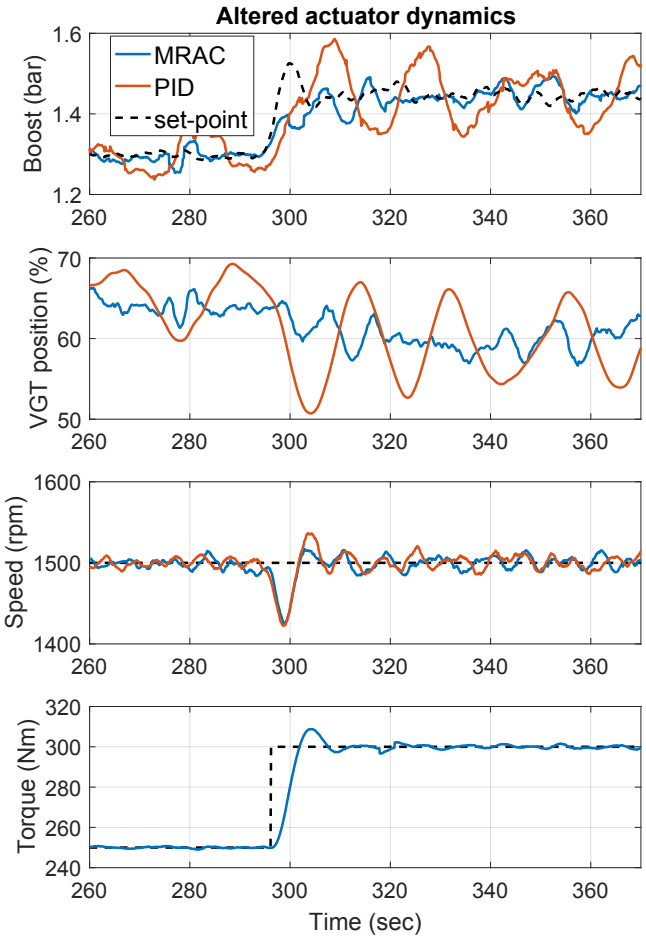

Fig. 17. Experimental results (realistic): MRAC vs PID under altered dynamics of the VGT actuator. The boost pressure set-point p_i^{sp} comes from the engine map $f(M_e, \omega_e)$. The load transient $250 \rightarrow 300$ Nm is shown @ 1500 rpm.

comparison for the previous test-run (Fig. 17). Significant oscillations of lambda λ^{PI} in the PI controlled engine are observed. Initial lambda undershoots for each of the controller (t=307 s for MRAC and t=314 s for PI) originate from the load overshoot during transient (see Fig. 17). After that, MRAC controlled engine demonstrates stable lambda (as expected from Fig. 17), while the PI becomes marginally stable with the second undershoot being even slightly higher than the first one (peak values for λ^{PI} can be seen in the figure).

VI. Conclusions

In this work, the indirect MRAC was proposed to successfully deal with controlling marine diesel engine under dynamic uncertainty originating from the mechanical wear of components. In order to tackle this problem, control adaptation to time-varying engine dynamics was proposed to maintain the nominal engine performance.

Numerical simulations showed that the proposed adaptive control system is stable and robust in the pres-

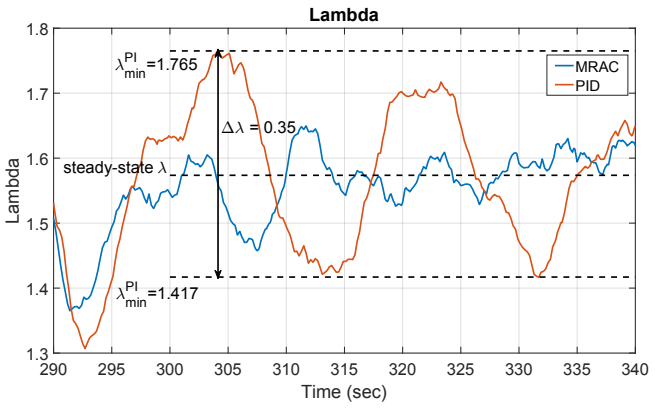

Fig. 18. Experimental results (realistic): Measured engine-out lambda comparison for adaptive and fixed-parameter control corresponding to the test-run in Fig. 17 (degraded actuator dynamics). It can be seen that oscillatory PI-controlled boost-pressure resulted in lambda oscillations with significantly greater amplitude than that of MRAC. Steady-state value of λ is evaluated as mean value of λ^{MRAC} with MRAC controlled engine. Peak values of λ^{PI} are also shown.

ence of uncertain actuator dynamics satisfying specified assumptions.

Eventually, the control system was validated with on-engine tests at the university engine laboratory. Realistic engine operating scenario was used during this validation phase with the constant speed, load transients and boost pressure set-point taken from the engine map.

ACKNOWLEDGMENTS

This research has received funding from the HERCULES-2 project, funded by the European Commission, DG Research, under Contract SCP1-GA-2011-284354.

NOMENCLATURE

Acronyms

CI	compression ignition
LP	linearization point
LTV	linear time-varying
MAP	manifold absolute pressure
MRAC	model reference adaptive control
OP	operating point
PE	persistently exciting
VGT	variable geometry turbocharger

Controller and identifier

$\alpha_1, \alpha_2, \beta_1, \beta_2$	parametrization of the numerator and denominator polynomials of the process
$\boldsymbol{\pi_0}$	estimate of $\boldsymbol{\pi}$ at previous time-instant
$\boldsymbol{\pi}$	vector of process parameters
$\boldsymbol{\theta}$	vector of process parameters
$\boldsymbol{\Xi}$	identifier tuning parameter
$\boldsymbol{b_\xi}$	identifier tuning parameter
$\boldsymbol{w}$	regressor vector
γ	identifier tuning parameter
ω_m	model natural frequency (tuning parameter)
σ	gain of the robustness modification of the identification algorithm
$\xi(s)$	arbitrary monic Hurwitz polynomial
ξ_1, ξ_2	coefficients of an arbitrary monic Hurwitz polynomial
ζ_m	model damping coefficient (tuning parameter)
a_1, a_2, b_1, b_2	time-domain process parameters (components of vector $\boldsymbol{\pi}$)
c_0, c_1, c_2, d_1, d_2	controller adaptive gains
d_m	denominator of the reference model transfer function
d_p	denominator of the process transfer function
$G(s)$	process transfer function
k_m	gain of the reference model transfer function
k_p	gain of the process transfer function
$M(s)$	reference model transfer function
n_m	numerator of the reference model transfer function
n_p	numerator of the process transfer function
p_i^{ident}	identified boost pressure, bar
p_1, p_2	poles of the process transfer function
u_{vgt}	VGT actuator commanded position
z_1	zero of the process transfer function
e	identification error, bar

Physical and geometrical quantities

δ_{vgt}	VGT position control increment, V
η	efficiency, %
$\gamma_c = c_{p,i}/c_{v,i}$	specific heat ratio
λ	air-fuel ratio
$\mu_c = (\gamma_c - 1)/\gamma_c$	constant
ω_e	engine speed, rad/s
$\psi(\cdot)$	flow correction coefficient
τ_c	turbocharger time-constant
τ_{act}	VGT actuator model time-constant
A_{vgt}	VGT effective area, m^2
$c_{p,i}$	gas specific heat constant, $\mathrm{J{\cdot}kg^{-1}K^{-1}}$
H_i	lower heating value of the fuel, MJ/kg
M_e	engine torque, Nm
M_l	load torque, Nm
N_e	engine rotational speed, rpm
P_c	compressor power, W
$p_{r,t}$	downstream to upstream pressure ratio
J	mass moment of inertia, $\mathrm{kg{\cdot}m^2}$
R	specific gas constant, $\mathrm{J{\cdot}kg^{-1}K^{-1}}$
T	temperature, K
V	manifold volume, m^3
W	mass flow, kg/s

Subscripts

a	ambient

c	compressor
e	engine
i	intake
is	isentropic
l	load
vgt	turbine
x	exhaust

REFERENCES

[1] F. Zhao, W. Yang, W. W. Tan, W. Yu, J. Yang, and S. K. Chou, "Power management of vessel propulsion system for thrust efficiency and emissions mitigation," *Applied Energy*, vol. 161, pp. 124–132, 2016.

[2] L. M. Eriksson and M. Johansson, "Pid controller tuning rules for varying time-delay systems," in *2007 American Control Conference*. IEEE, 2007, pp. 619–625.

[3] D. Yu, T. Chang, and D. Yu, "A stable self-learning pid control for multivariable time varying systems," *Control Engineering Practice*, vol. 15, no. 12, pp. 1577–1587, 2007.

[4] "International maritime organization, nitrogen oxides (nox) regulation 13." [Online]. Available: http://www.imo.org/en/OurWork/Environment/PollutionPrevention/AirPollution/Pages/Nitrogen-oxides-(NOx)-%E2%80%93-Regulation-13.aspx

[5] "Higher efficiency, reduced emissions, increased reliability and lifetime, engines for ships, 2012," see also URL `http://hercules-c.com`. [Online]. Available: http://http://hercules-c.com

[6] "Fuel flexible, near -zero emissions, adaptive performance marine engine, 2015," see also URL `http://cordis.europa.eu`. [Online]. Available: http://cordis.europa.eu/project/rcn/196603_en.html

[7] E. Sciberras and R. Norman, "Multi-objective design of a hybrid propulsion system for marine vessels," *Electrical Systems in Transportation, IET*, vol. 2, no. 3, pp. 148–157, 2012.

[8] P. Kaluza, A. Kölzsch, M. T. Gastner, and B. Blasius, "The complex network of global cargo ship movements," *Journal of the Royal Society Interface*, vol. 7, no. 48, pp. 1093–1103, 2010.

[9] D. Mavrakis and N. Kontinakis, "A queueing model of maritime traffic in bosporus straits," *Simulation Modelling Practice and Theory*, vol. 16, no. 3, pp. 315–328, 2008.

[10] P. Kujala, M. Hänninen, T. Arola, and J. Ylitalo, "Analysis of the marine traffic safety in the gulf of finland," *Reliability Engineering & System Safety*, vol. 94, no. 8, pp. 1349–1357, 2009.

[11] A. Kasper, S. Aufdenblatten, A. Forss, M. Mohr, and H. Burtscher, "Particulate emissions from a low-speed marine diesel engine," *Aerosol Science and Technology*, vol. 41, no. 1, pp. 24–32, 2007.

[12] S. Skogestad and I. Postlethwaite, *Multivariable feedback control: analysis and design*. Wiley New York, 2007, vol. 2.

[13] S. Sastry and M. Bodson, *Adaptive control: stability, convergence and robustness*. Courier Corporation, 2011.

[14] S. Samokhin, S. Topaloglou, G. Papalambrou, K. Zenger, and N. Kyrtatos, "Adaptive power-split control design for marine hybrid diesel powertrain," *Journal of Dynamic Systems, Measurement, and Control*, vol. 139, no. 2, p. 021012, 2017.

[15] C. Lynch, H. Hagras, and V. Callaghan, "Using uncertainty bounds in the design of an embedded real-time type-2 neuro-fuzzy speed controller for marine diesel engines," in *2006 IEEE International Conference on Fuzzy Systems*. IEEE, 2006, pp. 1446–1453.

[16] K. V. Nielsen, "Exhaust recirculation control for reduction of nox from large two-stroke diesel engines," Ph.D. dissertation, 2016.

[17] K. V. Nielsen, M. Blanke, and M. Vejlgaard-Laursen, "Nonlinear adaptive control of exhaust gas recirculation for large diesel engines," *IFAC-PapersOnLine*, vol. 48, no. 16, pp. 254–260, 2015.

[18] H. Tang, L. Weng, Z. Y. Dong, and R. Yan, "Adaptive and learning control for si engine model with uncertainties," *IEEE/ASME Transactions on Mechatronics*, vol. 14, no. 1, pp. 93–104, 2009.

[19] K. R. Muske, J. C. P. Jones, and E. Franceschi, "Adaptive analytical model-based control for si engine air–fuel ratio," *IEEE Transactions on control systems technology*, vol. 16, no. 4, pp. 763–768, 2008.

[20] J. Larimore, S. Jade, E. Hellström, L. Jiang, and A. G. Stefanopoulou, "Adaptive control of a recompression four-cylinder hcci engine," *IEEE Transactions on Control Systems Technology*, vol. 23, no. 6, pp. 2144–2154, 2015.

[21] Z. Qiu, M. Santillo, M. Jankovic, and J. Sun, "Composite adaptive internal model control and its application to boost pressure control of a turbocharged gasoline engine," *IEEE Transactions on Control Systems Technology*, vol. 23, no. 6, pp. 2306–2315, 2015.

[22] L. Guzzella and A. Amstutz, "Control of diesel engines," *Control Systems, IEEE*, vol. 18, no. 5, pp. 53–71, 1998.

[23] J. B. Heywood, *Internal combustion engine fundamentals*. Mcgraw-hill New York, 1988, vol. 930.

[24] L. Eriksson and L. Nielsen, *Modeling and control of engines and drivelines*. John Wiley & Sons, 2014.

[25] M. Jankovic and I. Kolmanovsky, "Robust nonlinear controller for turbocharged diesel engines," in *American Control Conference, 1998. Proceedings of the 1998*, vol. 3. IEEE, 1998, pp. 1389–1394.

[26] R. Lozano and R. G. Moctezuma, "Model reference adaptive control with unknown high frequency gain sign," *Automatica*, vol. 29, no. 6, pp. 1565–1569, 1993.

[27] P. Ioannou, "Robust adaptive controller with zero residual tracking errors," *IEEE Transactions on Automatic Control*, vol. 31, no. 8, pp. 773–776, 1986.

[28] P. Ioannou and K. Tsakalis, "A robust direct adaptive controller," *IEEE Transactions on Automatic Control*, vol. 31, no. 11, pp. 1033–1043, 1986.

[29] N. Cavina, E. Corti, and D. Moro, "Closed-loop individual cylinder air–fuel ratio control via uego signal spectral analysis," *Control Engineering Practice*, vol. 18, no. 11, pp. 1295–1306, 2010.